Performance of Tencate Mirafi PGM-G^4 Interlayer-Reinforced Asphalt Pavements in Alaska

Phase I Report

Submitted to
Tencate Geosynthetics North America

by

Peng Li, Ph.D.
Research Assistant
Department of Civil and Environmental Engineering

Jenny Liu, Ph.D., P.E.
Associate Professor
Department of Civil and Environmental Engineering

Paul Eckman
Undergraduate Research Assistant
Department of Civil and Environmental Engineering

August 2014

University of Alaska Fairbanks
Fairbanks, AK 99775-5900

EXECUTIVE SUMMARY

Geosynthetics has been used in hot mix asphalt (HMA) overlays in a variety of design and construction situations for more than three decades. A number of positive benefits have been identified such as waterproofing control for base and subgrade protection, improved fatigue resistance and reduced propagation of reflective cracks. In cold regions such as Alaska and other northern states, pavements are more prone to distresses due to extreme climatic conditions. Research is needed to explore how interlayers functions in asphalt pavements in cold regions.

The interlayers used for pavement reinforcement applications and available in the market are primarily biaxial. Biaxial grids with equal strength in both the machine and cross machine directions allow stress transfer at low strain mainly in longitudinal and transverse directions. The new PGM-G^4 paving composite developed by Tencate Geosynthetics contains multi-axial fiberglass filament yarn, which changes the aperture geometry from a rectangular to a quad angular grid structure. This unique feature improves the structure radial stiffness and efficiently distributes stress from surface layer to the geogrid throughout the full 360^o. This isotropic feature could deliver optimal asphalt concrete (AC)/grid interaction and more efficient reinforcement. There is a need to identify/validate its expected performance and added value over conventional biaxial grids.

Hence, a study has been conducted on interlayer-reinforced asphalt pavements in Alaska that included two phases: laboratory index testing (Phase I) and field performance evaluation (Phase II). Phase I focused on laboratory evaluation of engineering properties of PGM-G^4 composite paving grid-reinforced asphalt pavement structure and comparison with other types of interlayers. Five types of interlayers were evaluated in this study for various laboratory tests and they were PGM-G^4 (multi-axial composite grid), PGM-G100/100 and PGM-G50/50 (bi-axial composite grid), TruPave® (engineered paving fiberglass and polyester hybrid mat), and MPV500 (conventional polypropylene interlayer). The performance tests included asphalt retention and grab strength tests of interlayers, and shear strength, permeability and indirect tension (IDT) tests of interlayer-reinforced asphalt mixtures. Further, a typical Alaska flexible pavement structure was used, and pavement structure analyses and simulation were conducted by Bisar, Alaska Flexible Pavement Design (AKFPD) and ABAQUS programs to investigate the effects of paving interlayers on the pavement performance.

Within the scope of this study, test and analysis results were summarized as follows.

- Five interlayers were in the following order in terms of asphalt retention value with PG 64-34 binder from highest to lowest one: PGM-G100/100, PGM-G50/50, MPV500, TruPave®, and PGM-G^4.

- The breaking tensile loads of the saturated and unsaturated paving interlayers in grab strength tests showed that the highest breaking load was obtained on PGM-G100/100, which was mainly contributed by the three yarns of reinforcement fiberglass. PGM-G^4 had the second highest breaking load. All specimens showed an increase of breaking tensile load after saturation and PGM-G^4 had the highest strength increase after saturation.
- The shear test results indicated that optimum performance was maximized when the material was placed "glass-down" into the bitumen tack coat to achieve maximum interface bonding strength.
- Permeability tests were conducted using mixtures reinforced with three interlayers (i.e. PGM-G^4, PGM-G100/100, and PGM-G50/50), with results yielding approximately 1/10 of that of control mixture. The lowest permeability was obtained from PGM-G100/100 treated specimens, followed by PGM-G^4 treated specimens and PGM-G50/50 treated specimens. The permeability of specimens treated by the MPV500 and TruPave without tack coat oil was higher than those specimens with tack coat oil, but still lower than the control mixture.
- Interlayer treated mixtures had lower creep compliance than the control mixture. At 20^{o}C, PGM-G^4 treated specimen had the highest creep stiffness, which was doubled that of the control group. The reduction of creep compliance of interlayer treated specimens indicated that the applied load mostly was carried by interlayer and the load on the HMA was reduced. At low temperatures, contraction strain would be generated, especially for locations where cracks exist. Paving composite could provide extra resistance to the thermal contraction. Even after thermal cracks occurred, the asphalt saturated paving interlayer could maintain its integrity.
- The structure analysis based on Bisar program showed that maximum tensile strain in the pavement with paving interlayer was lower than pavement with control mix, indicating that using interlayer could improve fatigue crack resistance and extend service life. PGM-G100/100 treated HMA had the lowest tensile strain.
- The calculation of fatigue life (corresponding to the condition of fatigue cracking (bottom-up) covering 45% of the wheel path area) based on the AKFPD program also indicated that the fatigue life of pavements with paving interlayers were higher than that of pavements without an interlayer. The fatigue life of pavement with PGM-G100/100 composite grid was more than three time higher than the control HMA.
- The results from simulation by finite element method (FEM) indicated that the multi-axial fiber glass reinforced paving interlayer PGM-G^4 could improve the stress distribution more effectively than PGM-G50/50. The tensile strain on the bottom of PGM-G^4 treated pavement was only 20% of that of PGM-G50/50 treated pavement.

In summary, the results from Phase I study confirmed that adding a paving interlayer can increase pavement structure stiffness, greatly reduce the permeability and also provide good resistance to low temperature cracking and fatigue cracking. In addition, FEM simulation results

indicated that the multi-axial interlayer PGM-G^4 could improve the stress distribution more effectively than bi-axial composite grid as reflected by much lower maximum tensile strain on the bottom of AC layer.

As follow-up of Phase I study, field test sections were established in summer of 2013. Results based on on-going field evaluation and data collection will further validate findings summarized from Phase I.

TABLE OF CONTENTS

LIST OF FIGURES

LIST OF TABLES

CHAPTER 1 INTRODUCTION

PROBLEM STATEMENT

Paving interlayers have been used in asphalt overlays in a variety of design and construction situations for more than three decades. A number of positive benefits include waterproofing control against infiltration of free surface water through the pavement into the base and subgrade soils; retarding of reflection of existing cracks and distresses; and providing for more stable subgrade moisture contents (Button 1989, Saraf et al. 1996, Chang et al. 1999, Khodaii and Fallah 2008, Chowdhury et al. 2009). Many references reported that the inclusion of a paving interlayer system significantly improved the performance of asphalt concrete (AC) overlays. This performance improvement was generally attributed to the waterproofing capabilities and the stress-absorption capabilities of the interlayer.

The interlayers primarily used for pavement reinforcement application and available in the market are manufactured as bi-axial (Figure 1.1a). Bi-axial grids with equal strength in both the machine and cross machine directions allow stress transfer mainly in longitudinal and transverse directions. The new PGM-G^4 interlayer developed by Tencate Geosynthetics with multi-axial grids (Figure 1.1b) changes the aperture geometry from a rectangular to a quad angular grid structure, which has the capability to provide a new level of in-plane radial stiffness – distributing radial stresses from AC layer to geogrid throughout the full 360^o. It is expected that this unique feature will deliver optimal AC/grid interaction and more efficient reinforcement, which leads to lower cost, longer lasting and more reliable asphalt pavements by improving performance, increasing service life, and extending maintenance and rehabilitation intervals. There is a need to identify/validate its expected performance and added value over the conventional biaxial grids. In addition, in cold regions such as Alaska and other northern states, pavements are more prone to distresses due to extreme climatic conditions. Research is needed as well to explore how this new type of interlayer functions in asphalt pavements in cold regions.

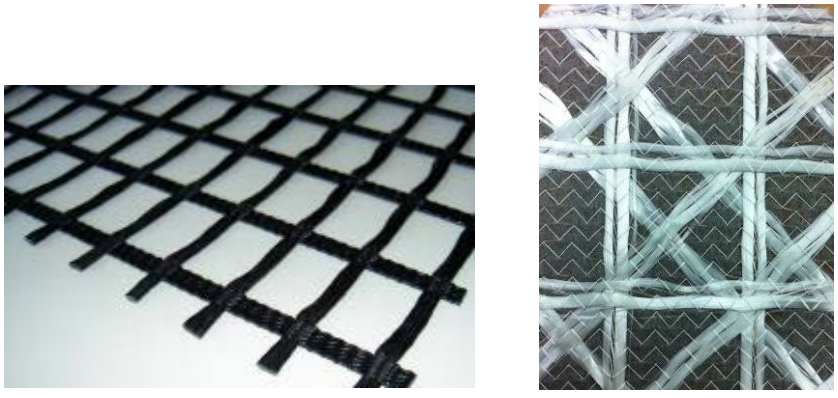

(a) (b)

Figure 1.1 (a) Bi-axial grid; (b) Multi-axial PGM-G^4 composite paving grid

OBJECTIVES

The following objectives were addressed in this study:

- To assess the engineering properties of PGM-G^4 composite paving grid-reinforced asphalt pavement structure in the lab,
- To predict overall asphalt pavement service life with the use of PGM-G^4 composite paving grid,
- To evaluate the effect of PGM-G^4 composite paving grid as an interlayer on the overall asphalt pavement performance in the field, and
- To provide recommendations for use of PGM-G^4 composite paving grid in asphalt paving and preservation projects in Alaska.

This study included two phases: laboratory index testing (Phase I) and field performance evaluation (Phase II). Phase I focused on laboratory evaluation of engineering properties of PGM-G^4 composite paving grid-reinforced asphalt pavement structure and comparison with other types of interlayers, as presented in this report. Chapter 2 presents a description of the laboratory testing methods, test procedures and results, and findings. Further analysis using pavement software and numerical simulation using finite element method (FEM) software package are summarized in Chapter 3. Conclusions are provided in Chapter 4.

CHAPTER 2 LABORATORY PERFORMANCE TESTS

TESTS OF INTERLAYERS

Materials

Five types of interlayers were evaluated in this study and they were PGM-G^4 (multi-axial composite grid), PGM-G100/100 and PGM-G50/50 (bi-axial composite grid), TruPave® (engineered paving fiberglass and polyester hybrid mat), and MPV500 (conventional polypropylene interlayer) (Figure 2.1).

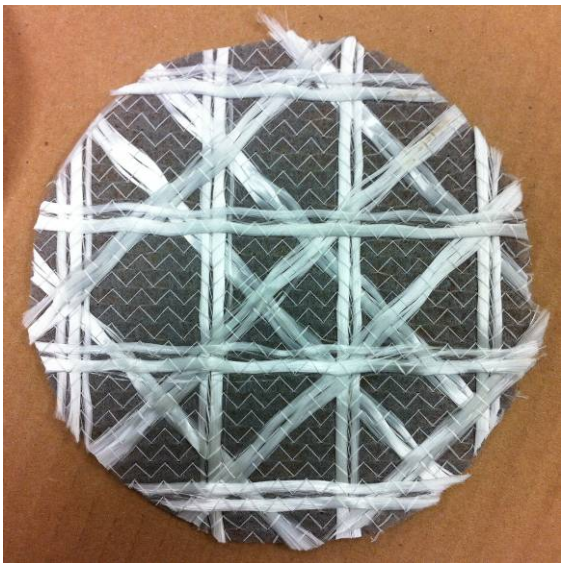

a) PGM-G^4

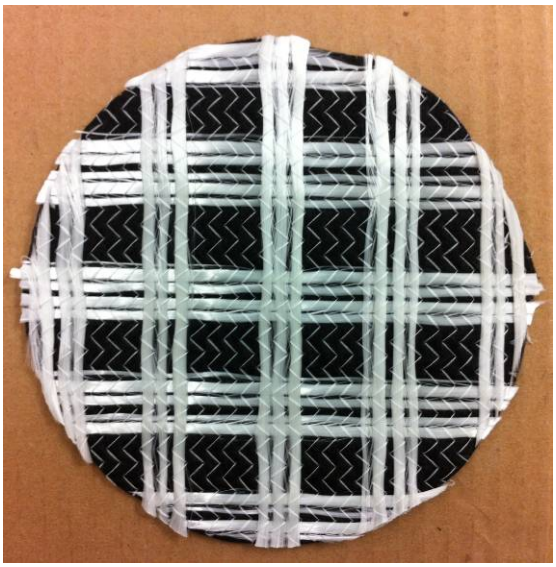

b) PGM-G100/100

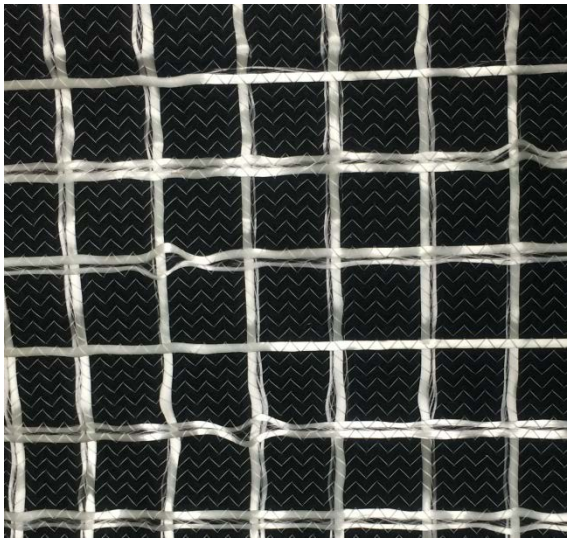

c) PGM-G50/50

d) TurPave®

e) MPV500

Figure 2.1 Paving interlayers used for specimen fabrication

Asphalt Retention of Interlayers

The asphalt retention tests were performed on five types of paving interlayers (PGM-G^4, PGM-G100/100, PGM-G50/50, TruPave® and MPV500) according to ASTM D6140. PG 64-34 modified binder was used. The conditioning temperature (135^{o}C) in ASTM D6140 is set for neat asphalt binders. Due to higher viscosity of modified binder, the conditioning temperature was increased to 145^{o}C. This temperature was chosen according to the compaction temperature specified in the JMF, in which PG 64-34 modified binder was used.

Interlayers including PGM-G100/100, PGM-G50/50, TruPave® and MPV500 were cut into the sizes of 4 inches in width and 8 inches in length according to the specified specimen size in ASTM D6140. The width of 4-in approximately covers three grid apertures for PGM-G100/100 and PGM-G50/50, but only covers two and half for G^4. Therefore, the width of G^4 samples was increased to 4.8 in. Four replicates were made for each type of interlayer. The weight of each specimen was measured and recorded. Specimens were then submerged in the asphalt binder for 30 minutes at 145^{o}C. After required submersion, saturated specimens were hung in the oven at 145^{o}C for 30 minutes and then rotated 180^o and hung for additional 30 minutes (Figure 2.2). The weights of saturated specimens were measured and recorded again. The asphalt retention was calculated according to the equation provided in ASTM D6140.

Figure 2.2 Asphalt retention test

Table 2.1 summarizes the asphalt retention results for all five interlayers. It can be seen that these five interlayers are in the following order in terms of asphalt retention value from highest to lowest one: PGM-G100/100, PGM-G50/50, MPV500, TruPave®, and PGM-G^4. Compared with the previous asphalt retention test with PG 52-28 binder under conditioning temperature of 135^{o}C, PGM-G^4 provided higher asphalt retention value with PG 64-34 binder under conditioning temperature of 145^{o}C (0.183 gl/yd^2 vs. 0.152 gl/yd^2). According to the visual observation, at 145^{o}C the modified binder (PG 64-34) was still viscous, leading to more retention of asphalt.

Table 2.1 Summary of asphalt retention (PG 64-34, 145^{o}C)

	PGM-G^4	PGM-G50/50	PGM-G100/100	TruPave®	MPV500
Asphalt Retention (gl/yd^2)	0.183	0.273	0.283	0.220	0.270

Grab Strength Tests of Interlayers

Grab strength tests were performed to measure the breaking load of interlayers. Saturated PGM-G^4 interlayers were cut into the size of 1.6 in. by 8 in. and other interlayers were cut in the size of 1 in. by 8 in. The grab strength is important to constructability and performance of water barrier

and reflective cracking control. Strong interlayer would benefit the pavement performance under a high traffic loading and in a cold climate. Table 2.2 summaries the braking tensile load of saturated and unsaturated paving interlayers. The highest breaking load was obtained on PGM-G100/100, which was mainly contributed by three yarns of reinforcement fiberglass. PGM-G^4 had the second highest breaking load. All specimens showed an increase of breaking tensile load after saturation and PGM-G^4 had the highest strength increase after saturation.

Table 2.2 Saturated vs. unsaturated breaking tensile load (lb) (*from Tencate*)

Type	PGM-G50/50	PGM-G^4	PGM-G100/100	TruPave®	MPV500
Testing Method	ASTM D6037 (Type A)	ASTM D6037 (Type A)	ASTM D6037 (Type A)	ASTM D5035	ASTM D5035
Saturated	454.7	514.8	915.3	53.2	73.4
Unsaturated	433	436.3	850.5	50.6	35.1
% Difference	5%	18%	8%	5%	109%

The results also indicated that the grab strength of fiberglass reinforced interlayer was mainly contributed from fiberglass. As the yarn of fiberglass increased, the strength increased. In addition, during testing, the tensile load was applied along the direction of fiberglass. For conventional biaxial composite, PGM-G100/100 and PGM-G50/50, if the loading direction was 45^o to the direction of fiberglass, their grab strength would be much lower, because there was not fiber glass installed in this direction. Meanwhile, PGM-G^4 with multi-axial fiberglass could provide same grab strength in 45^o direction which enable more efficient stress distribution within the pavement structure.

TESTS OF HMA MIXTURES WITH INTERLAYERS

Materials

The HMA was laboratory blended mixtures according to the job mix formula (JMF) used for Rich Hwy North Pole Interchange paving project located in North Pole, Alaska. The JMF was designed according to Marshall mix design method. PG 64-34 Binder was used. The aggregate and binder were collected form the same resources as used in the paving project. The details of JMF can be found in Appendix.

Shear Test

Specimens Preparation

The shear tests were performed to measure the shear strength among the interface between layers. Four types of paving interlayers were used, including PGM-G^4, PGM-G100/100, TruPave® and MPV500. There were six types of specimens listed in Table 2.3 and three replicates were made for each type of specimen. Two types of specimens were made for both PGM-G^4 and PGM-G100/100 paving interlayers with tack coat binder applied to either glass side or nonwoven side during the compaction. By comparing the results from these two types of specimens, one could determine the best way to place the interlayer in the pavement to ensure strong bonding between paving interlayer and AC.

Table 2.3 Summary of testing specimens

No	**Interlayer**	**Tack Coat Binder**	**Placement of Interlayer**	**Loading Condition**
1	PGM-G^4	PG 64-34	tack to glass side	load from nonwoven side
2	PGM-G^4	PG 64-34	tack to nonwoven side	load from glass side
3	PGM-G100/100	PG 64-34	tack to glass side	load from nonwoven side
4	PGM-G100/100	PG 64-34	tack to nonwoven side	load from glass side
5	TruPave®	PG 64-34	tack to fussy side	load from top half of specimen
6	MPV500	PG 64-34	tack to fussy side	load from top half of specimen

Specimens were compacted using Superpave Gyratory Compactor (SGC). Specimens were 120 mm in height and 150 mm in diameter. The paving interlayer was place in the middle of specimen. The number of gyration was adjusted according to the target air voids of 4% listed in the JMF. The trial tests were performed without paving interlayer. It was assumed that under same compaction effort, the specimens with paving interlayer would achieve same air void content as the one without interlayer. The tack coat application rate for each interlayer is listed in Table 2.4. The weight of binder used for each specimen was calculated based on the shooting rate, cross section area (27.4 in^2), and binder specific gravity (1.0016 g/cm^3).

Table 2.4 Tack coat application rates

Interlayer	Shooting Rate (gal/yd^2)	Weight for Each Specimen (g)
PGM-G^4	0.19	15.2
PGM-G100/100	0.27	21.6
TruPave®	0.20	16.0
MPV500	0.25	20.0

The specimens were compacted in three steps:

- Step 1: Compact first half specimen as shown in Figure 2.3.
- Step 2: Apply tack coat and place the paving interlayer. The tack coat binder (PG 64-34) was applied on the surface of first half specimen according to the application rates listed in Table 2.4. Then paving interlayer was placed on top of the tack coat binder (Figure 2.4).
- Step 3: the rest of loose mixture was loaded and final compaction was completed (Figure 2.5).

a) Load loose mixture

b) Finished first half specimen (inside the mold)

Figure 2.3 Compact first half of specimen

a) Tack coat

b) Paving interlayer

Figure 2.4 Tack coat and paving interlayer

a) Final compaction b) Fresh specimen

Figure 2.5 Final compaction

Tests and Results

The shear tests were performed in a computer controlled close-loop hydraulic loading system. The specimen was hold in a shear testing fixture as shown in Figure 2.6. During the test, the vertical load was transformed into a shear force through the shear testing fixture. As illustrated in Figure 2.6, the vertical load was applied on the second half of compacted specimens, which simulated the traffic loading condition in the field. The detailed loading conditions are listed in Table 2.3, e.g. for PGM-G[4] treated specimens, when the tack coat was applied to glass side, the load was applied from the nonwoven side. The vertical load was applied on the top part of the specimens at the rate of 12.5 mm/min until specimens were sheared apart.

After shear tests, all specimens were sheared off along the glass side of interlayer indicating the interface between glass side and HMA was the weak side (Figure 2.7). Based on such observation, the interlayer needs to be placed with glass side facing down to have a direct contact with tack coat to improve the bonding strength.

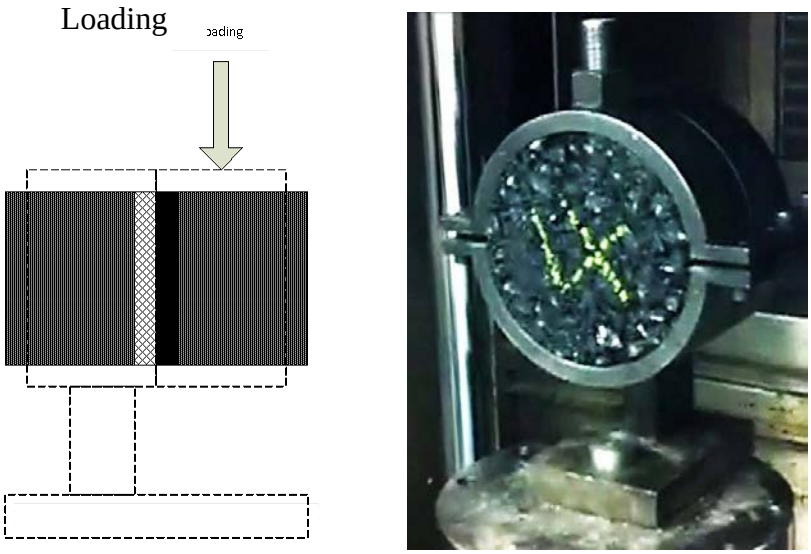

a) Sketch b) Specimen installation

Figure 2.6 Shear testing setup

a)PGM-G^4 b) PGM-G100/100

Figure 2.7 Specimens after shear testing

The shear strength results are summarized in Figure 2.8. For PGM-G^4 and PGM-G100/100 treated specimens, "_G" stands for that the glass side of interlayer was facing down during compaction, and "_N" stands for that nonwoven side of interlayer was facing down. It can be seen that the specimens with glass side of interlayer facing down had the higher shear strength and the value could be up to 80% higher than the strength of specimens with nonwoven side facing down. Therefore, during the field application, the interlayers need to be placed glass side facing down to achieve the maximum interface bonding strength. In addition, specimens with

PGM-G[4] interlayer, which had less fiberglass, had higher shear strength than those with PGM-G100/100. Fiberglass could only absorb a little asphalt and its surface was slippery, which provided less shear resistant and bonding strength than nonwoven materials.

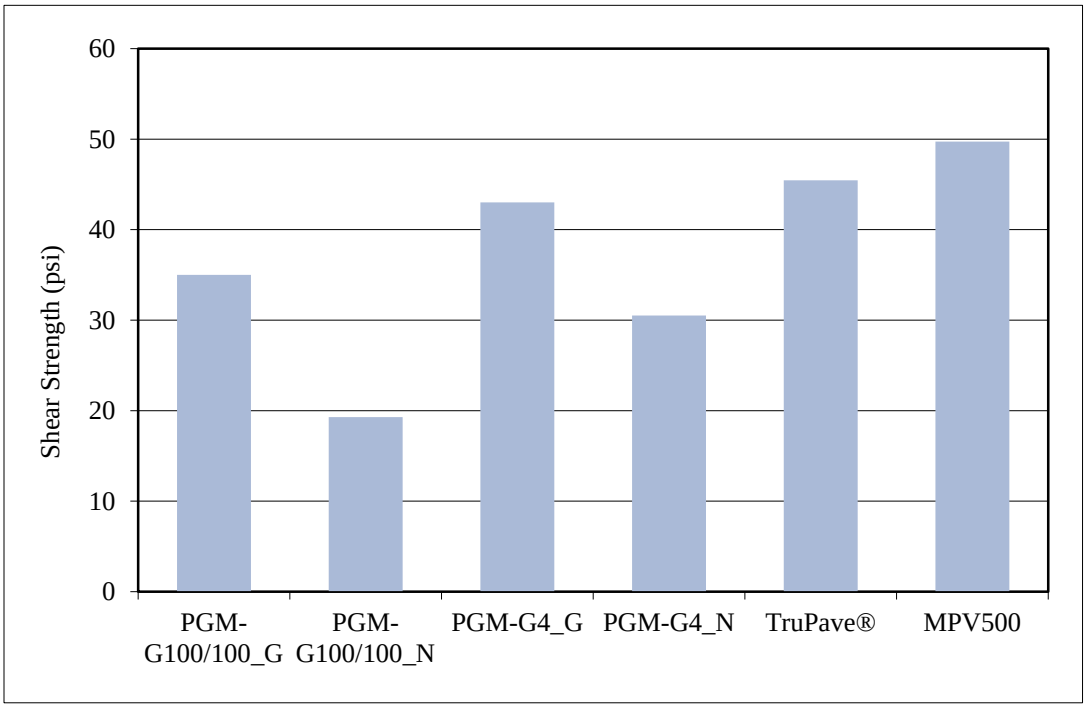

Figure 2.8 Summary of shear strength results

Permeability Test

Permeability, or coefficient of permeability, is the rate at which a porous material will transmit water under a hydraulic gradient. It is an important property of HMA, which highly correlates to the moisture susceptibility and durability of asphalt pavement. The recommended maximum acceptable permeability is 125×10^{-5} cm/s (Maupin 2000). The permeability tests were performed using a flexible wall permeameter according to ASTM PS 129-01 (2004). The control group was regular HMA without paving interlayer. According to the recommendation from Georgia DOT (2011), the specimens with the height of 75 mm and target air void of 6% were compacted using the same process as the one used for shear test. Figure 2.9 shows the testing setup for the permeability test. Before testing, the specimen was saturated using vacuum. Then, it was taken out and the surface of the specimen was dried using a towel. The petroleum jelly was applied on the side of specimen for sealing to prevent water leaking from the side of the specimen. When the specimen and permeameter was assembled, water was filled into the plastic tube to reach the 500 cm^3 mark (62 cm in height, h_1). Then the draining valve was opened. After 30 min, the water head was read and recorded as h_2. The test was performed twice on the same specimen.

Figure 2.9 Permeameter

The permeability was calculated based on Darcy's law as shown in Eq. 1.

$$k = \frac{aL}{At} \ln\left(\frac{h_1}{h_2}\right) t_c \quad \text{.....(1)}$$

where,

k = coefficient of water permeability, cm/s,
a = inside cross-sectional area of inlet standpipe, cm^2 (7.92 cm^2),
L = average thickness of test specimen, cm,
A = average cross-sectional area of test specimen, cm^2 (176.7 cm^2),
t = average elapsed time of water flow between timing marks (h_1 and h_2), s,
h_1 = hydraulic head on specimen at time t_1, cm,
h_2 = hydraulic head on specimen at time t_2, cm, and
t_c = temperature correction for viscosity of water (1.0 for 20°C).

Figure 2.10 summarizes the effect of paving interlayers on permeability of HMA. The permeability values of all specimens were less than the recommended maximum acceptable permeability, 125×10^{-5} cm/s. The average permeability of control group is 18.5×10^{-5}cm/s. The paving interlayer greatly reduced the permeability of HMA specimen. The permeability of specimens treated with three interlayers (i.e. PGM-G^4, PGM-G100/100, and PGM-G50/50) was

about 1/10 of that of control group. The lowest permeability was obtained from PGM-G100/100 treated specimens, followed by PGM-G^4 treated specimens and PGM-G50/50 treated specimens. The permeability of specimens treated by the MiraPave and TruPave® without tack coat oil was higher than those specimens with tack coat oil, but still lower than the control group. The improvements of water resistance of MiraPave and TruPave® treated specimens were mainly contributed by the adhesive layer that was applied on the paving interlayer.

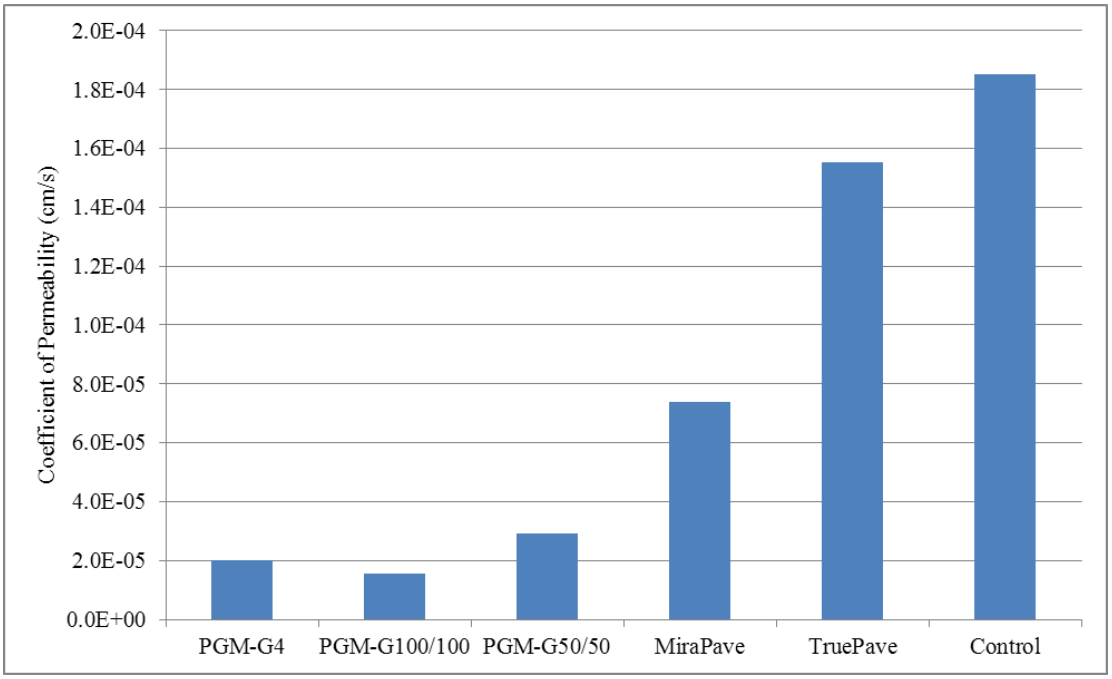

Figure 2.10 Permeability testing results

Indirect Tension Test

Indirect tension (IDT) creep tests were performed on control HMA (without paving interlayer), PGM-G^4, PGM-G100/100, and PGM-G50/50 treated specimens at 20^{o}C, -10^{o}C and -30^{o}C to evaluate low temperature performance of mixtures. The specimen fabrication process was the same as the one used for the shear test, except that specimens were cut into the thickness of 50 mm. As shown in Figure 2.11, a vertical load was applied along the radial direction of the specimen, and a horizontal tensile stress was generated in the center of the specimen during the testing. A constant load of 12 kN, 1.5 kN and 0.15 kN were used at -30^{o}C, -10^{o}C and 20^{o}C, respectively. The total loading period was 1000 seconds.

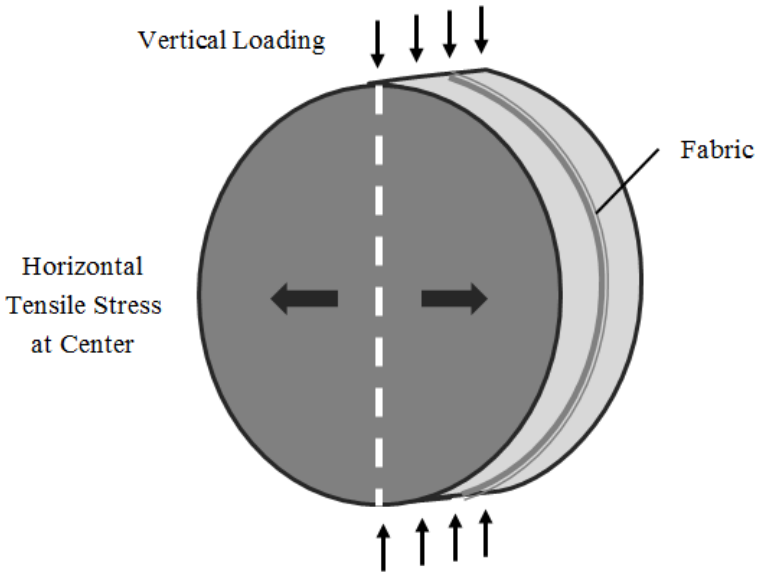

Figure 2.11 Sketch of IDT test

The creep compliance is a viscoelastic property of HMA. It is used in the mechanistic empirical flexible pavement design guide (MEPDG) to calculate the thermal stress at low temperatures. For certain stress, the creep compliance can be determined as the ratio of strain to stress at a certain time. The creep compliances at different loading temperatures obtained from IDT creep tests are summarized in Table 2.5. In general, interlayer treated specimens had lower creep compliances than control materials. At 20°C, PGM-G[4] treated specimen had the lowest creep compliance, which was only about half of that of control group. At the lower temperatures, i.e. -10°C and -30°C, the creep compliance of three types of interlayer treated specimens were close.

Table 2.5 Summary of creep compliance (1/MPa)

Temperature (°C)	Material	Time (s)						
		10	20	50	100	200	500	1000
20	Control	4.90	18.39	46.22	68.08	90.64	121.33	145.55
	PGM-G[4]	5.23	12.31	25.03	35.19	46.20	63.59	78.94
	PGM-G50/50	7.96	19.87	34.17	44.58	55.30	70.97	83.98
	PGM-G100/100	5.09	14.54	30.74	44.70	60.00	82.36	100.45
-10	Control	0.27	0.34	0.60	1.04	1.31	1.71	1.84
	PGM-G[4]	0.19	0.26	0.52	0.81	1.00	1.16	1.23
	PGM-G50/50	0.19	0.26	0.45	0.70	0.90	1.11	1.24
	PGM-G100/100	0.14	0.19	0.40	0.63	0.82	0.97	1.06
-30	Control	0.09	0.09	0.11	0.14	0.17	0.20	0.20
	PGM-G[4]	0.06	0.07	0.08	0.11	0.15	0.17	0.16
	PGM-G50/50	0.05	0.05	0.07	0.10	0.14	0.16	0.17
	PGM-G100/100	0.05	0.05	0.06	0.09	0.13	0.15	0.15

The viscoelastic behavior of HMA is dominated by temperature. It can be seen from Figure 2.12 that as temperature dropped from 20°C to -30°C, the creep compliance decreased more than 400 times for all mixtures. HMA with lower creep compliance and lower creep rate would be more prone to low temperature cracking. Though all mixtures showed decreased creep compliance with the decrease of temperature, at very low temperatures, the mixtures with paving interlayers had comparable creep compliances compared with the control mixtures. On the other hand, adding paving interlayer to HMA greatly reduced the temperature sensitivity of the material, especially for PGM-G[4], which was mainly contributed by the multi-axial fiberglass.

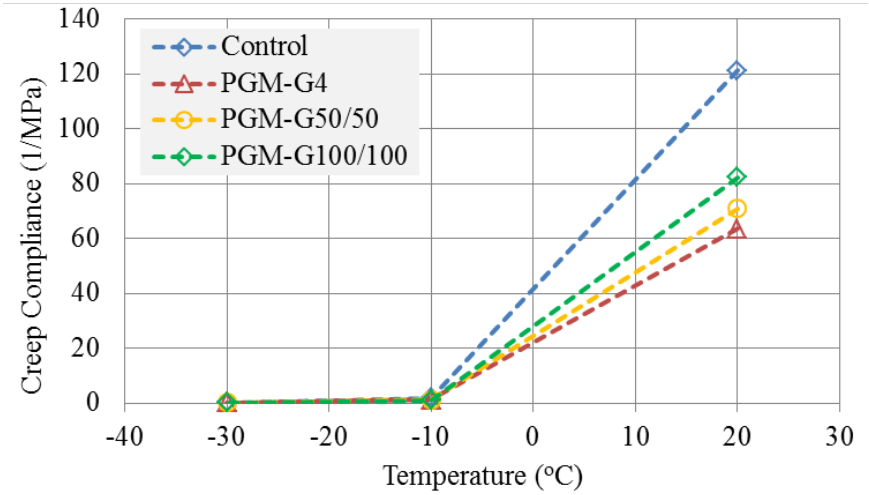

Figure 2.12 Effect of temperature on creep compliance (500s)

In cold regions, asphalt pavement suffers from low temperature cracking due to thermal contraction. HMA with higher creep compliance and higher creep rate would be less prone to low temperature cracking. However, it is worth noting the creep compliance of interlayer treated specimens was the combination of HMA and saturated paving interlayer. The creep compliance and strength of HMA itself would not change since the interlayer was only placed at the interface. The reduction of creep compliance of interlayer treated specimens indicated that the applied load mostly was carried by interlayer and the load on the HMA was reduced. Figure 2.13 shows the creep curves of horizontal tensile strain for four types of material at three different temperatures (i.e. 20°C, -10°C and -30°C). At 20°C, the creep strain of PGM-G[4] treated HMA was about half of the control group's strain at the end the test. At lower temperatures, i.e. -10°C and -30°C, the creep strain of interlayer treated specimens were at least 10% lower than the control group's strain. In addition, the effect of adding interlayer was more significant as loading time increased. At the beginning of the test (within initial 50 seconds), all the curves almost overlapped on each other, indicating that saturated paving composite had lower creep rate and the difference of creep rate between HMA and paving composite could be the primary reason for the reduction of creep strain on the treated specimens.

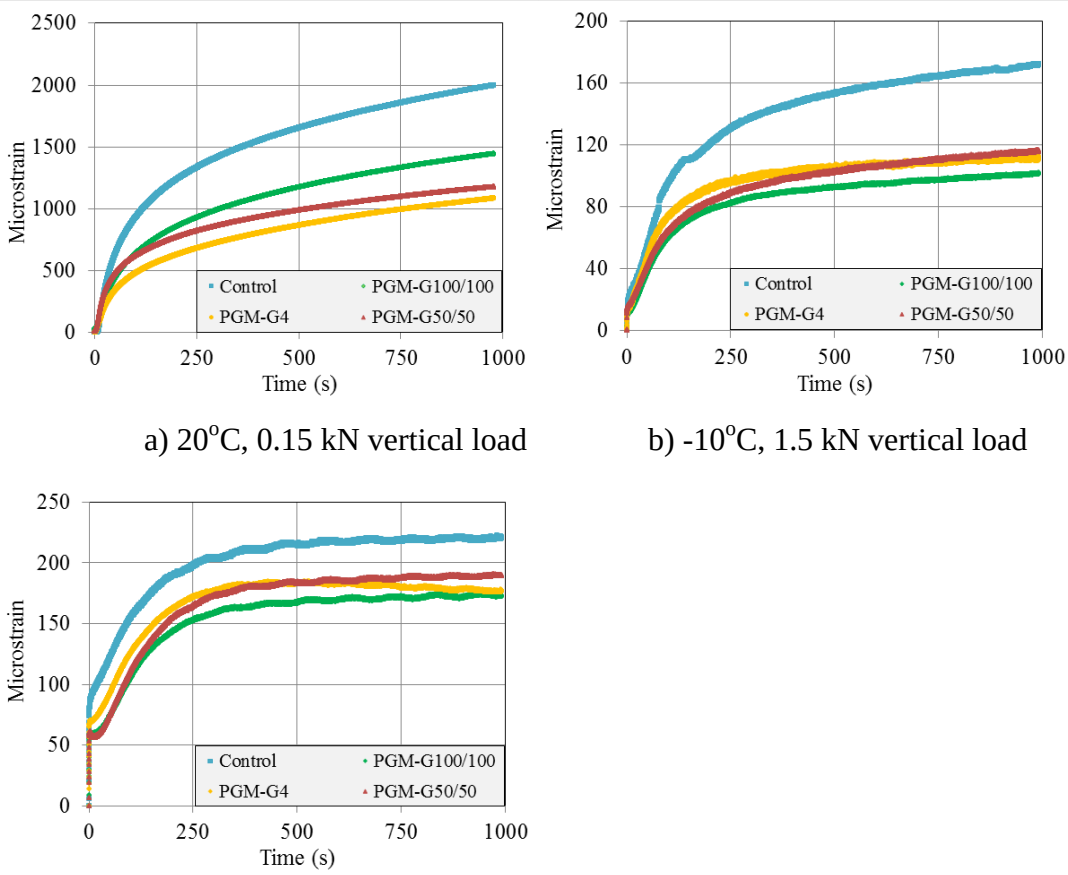

a) 20°C, 0.15 kN vertical load

b) -10°C, 1.5 kN vertical load

c) -30°C, 12 kN vertical load

Figure 2.13 Summary of horizontal creep strain

In the field, for pavement without any cracks, which can be considered as an infinite band structure along the direction of the road, low temperature would only impose thermal stress on the pavement but not thermal contraction strain. Therefore, adding paving interlayer may not contribute to thermal cracking resistance. However, contraction strain would be generated under low temperature, especially for locations where cracks exist. In this case, fiberglass reinforced paving interlayer could provide extra resistance to the thermal contraction. Even after thermal cracks occurred, the asphalt saturated paving interlayer could maintain its integrity and continue to provide a moisture barrier to the underlying pavement.

Dynamic Modulus

The mechanical-empirical pavement design guide (MEPDG) uses dynamic modulus (|E*|) of HMA in the structural analysis to calculate stresses, strains and displacements of flexible

pavement under various loading and climate conditions. |E*| is the absolute value of complex modulus (E*), which is a complex number and defines the relationship between stress and strain under sinusoidal loading for linear viscoelastic materials. The dynamic modulus is determined by applying sinusoidal loads to specimen while measuring the deformation. Then the |E*| is calculated by dividing the stress amplitude by the strain amplitude (Eq. 2).

$$|E^*| = \frac{\delta_0}{\varepsilon_0} \quad (2)$$

where,

|E*| = dynamic modulus, MPa,

σ_0 = peak-to-peak stress amplitude, MPa, and

ε_0 = peak-to-peak strain amplitude.

The dynamic modulus |E*| tests were performed for four types of asphalt mixtures, including a control mix, and PGM-G50/50, PGM-G100/100, and PGM-G[4] treated HMAs. Cylindrical specimens with 100 mm in diameter and 150 mm in height were used. The interlayers were horizontally placed in the middle of the specimen. Specimens were compacted using the SGC, and the procedure was the same as that used for shear test specimens. The raw size of compacted specimens was 180 mm in height and then they were cut and cored into the required size. The target air voids of testing specimens were 4%. Trial compactions were conducted to determine the number of gyration, at which the target air voids could be achieved. The total number of gyration was determined to be 10.

To take into account the time-temperature dependence of |E*|, usually the test is performed at four temperatures (i.e. 4^{o}C, 21^{o}C, 37^{o}C, and 54^{o}C) and at least six frequencies (i.e. 0.1, 0.5, 1.0, 5, 10, and 25 Hz) (AASHTO TP62). Using the principle of time-temperature superposition, a master curve is constructed by shifting the data at various temperatures to the reference temperature (usually 21^{o}C) with respect the time until the curves merge into a single smooth function.

The |E*| tests were performed on the asphalt mixture performance tester (AMPT). The AMPT is a computer–controlled hydraulic testing system capable to apply cyclic/static loading over a range of temperatures and frequencies/time on compacted HMA specimen. The machine consisted of a triaxial cell, an environmental chamber, a hydraulic actuator and pump, a temperature control unit and a data acquisition system (Figure 2.14). The triaxial test cell is mounted on the top left of the unit. For |E*| tests, the deformation is measured by 3 LVDTs attached on the side of specimens. External compressed air supply is required to apply confining pressure (in this study, the confining pressure was not used for |E*| tests) and to raise and lower

the triaxial cell. The integrated data acquisition and analysis software automatically process measurements and calculated |E*| at each loading frequency.

Figure 2.14 Setup of the AMPT

The rheological properties of HMA mixtures, such as |E*|, depend on both temperature and loading frequency. It also has been found that time temperature superposition principle can be applied for asphalt mixture, since it is a linear viscoelastic material, which means the modulus measured at the higher temperature and the lower loading frequency equals to the one measured at lower temperature and higher frequency. Therefore, usually, the |E*| of HMA is characterized over a wide range of loading time or frequency (10^{-4} to 10^{4} s or Hz). However, due to the practical limitation of machine's capacity, the loading frequency applied during test only goes up to 25 Hz. This limited range of loading frequency is extended by using the time temperature superposition principle. |E*|values measured over a range of temperatures and loading frequencies can be shifted with respect to frequency/time axis to form a smooth "S" shape curve at a reference temperature (usually 20^{o}C). This curve is called master curve of |E*|. The |E*| master curve is used in the MEPDG for structural analysis and to account for temperature and frequency effects of asphalt mixtures at all analysis levels.

Master curves of all mix investigated in this study were generated and summarized in Figure 2.15. It can be seen that master curves of all interlayer treated specimens were lower than the master curve of control mix, indicating that interlayer treated specimens had lower |E*|. The measured |E*| was the modulus of the entire system composed of HMA and asphalt saturated

interlayer. Due to the high binder content, the saturated paving interlayer was very soft and led to the low |E*| of the interlayer treated specimens. The master curves of PGM-G50/50 and PGM-G^4 treated specimens almost overlapped on each other. PGM-G100/100 treated specimens had the lowest |E*|.

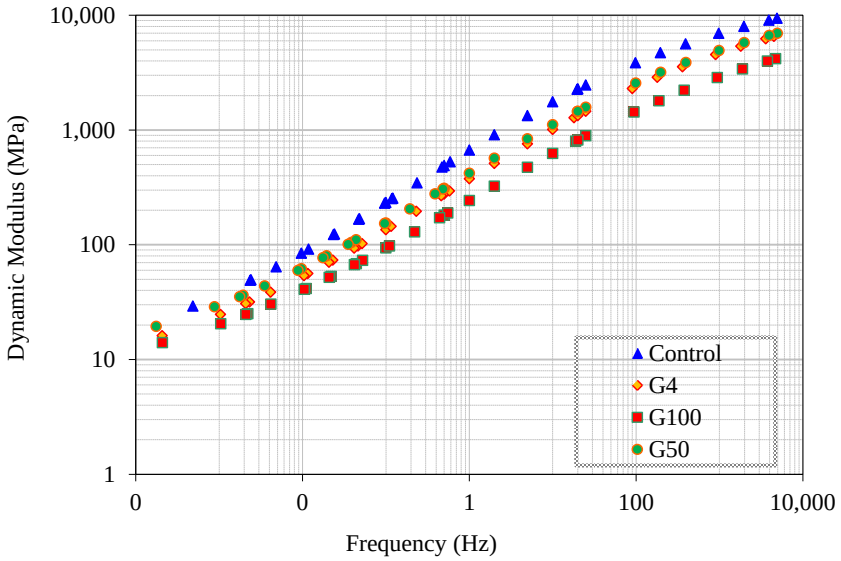

Figure 2.15 Master curves of |E*|

CHAPTER 3 PAVEMENT STRUCTURAL ANALYSIS

In addition to the laboratory tests, pavement structural analysis by several pavement analysis programs and numerical simulations was conducted to evaluate the performance of interlayer-reinforced AC pavements. Analyses and results are presented in this chapter.

MEPDG ANALYSIS

To further evaluate the effect of paving interlayers on the overall AC pavement performance, the MEPDG program was used to predict the overall asphalt pavement service life. The |E*| master curves of asphalt mixtures are the necessary material input in the MEPDG program. A typical Alaska flexible pavement structure was used. The pavement consisted of 2 in HMA surface layer, 4 in aggregate base, 24 in aggregate subbase (with lower quality aggregate) and subgrade. The moduli of base, subbase and subgrade are 45 ksi, 29 ksi and 14.5 ksi, respectively. The measured |E*|s were used as inputs of moduli for HMA surface layer. The HMA and paving interlayer was considered as one layer. The pavement was expected to last 15 years with AADT of 2500 and growth rate of 4%. However, due to the extremely low |E*| of interlayer-treated specimens, which exceed the lower limit of input for MEPDG (10 ksi), the program could not accept these values.

BISAR ANALYSIS

Since the analysis could not be performed for pavement with interlayer-treated HMA in MEPDG, Bisar, a program based on conventional linear elastic layered system was used for structure analysis. The |E*|s measured at 21^{o}C under a loading frequency of 10 Hz was used as moduli of surface layer. For HMA, most design methods (including MEPDG) use the maximum tensile strain at the bottom of HMA layer as a critical pavement response to estimate fatigue cracking. Maximum tensile strain at the bottom of surface layer was collected from pavements with four types of materials investigated in this study. The results are shown in Figure 3.1. Maximum tensile strain in the pavement with paving interlayers was lower than that of pavement with control mix, indicating that adding interlayers could improve pavement crack resistance and extend service life. PGM-G100/100 treated HMA had the lowest tensile strain.

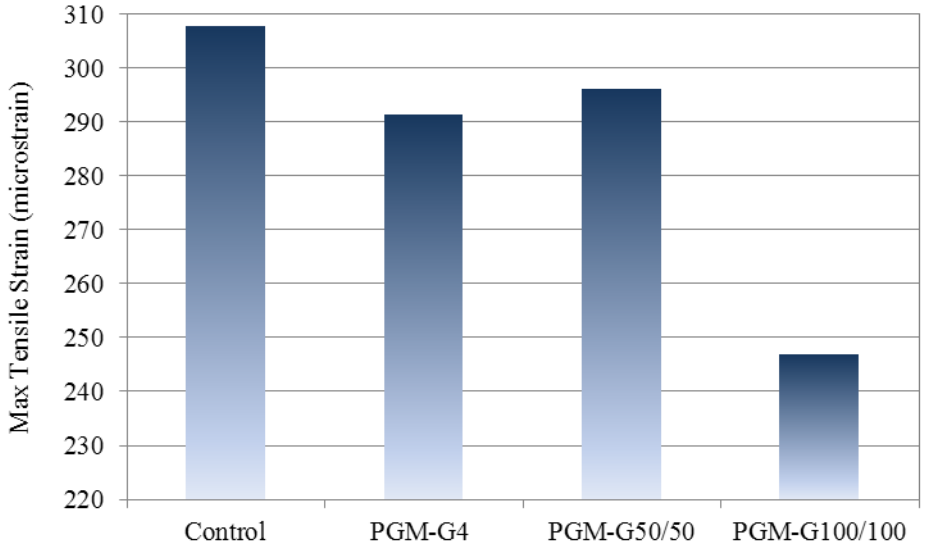

Figure 3.1 Maximum tensile strain at the bottom of surface layer

AKFPD ANALYSIS

In the Alaska Flexible Pavement Design (AKFPD) Program, maximum horizontal tensile strain at the bottom of specified layers, one of the critical pavement responses, is selected from structure analysis results and substituted into the fatigue failure model (Eq. 3) to calculate the fatigue life corresponding to the condition of fatigue cracking (bottom-up) covering 45% of the wheel path area.

$$N_f = C \times 0.07958 \times {\varepsilon_h}^{-3.291} \times |E^*|^{-0.854} \quad (3)$$

$$C = 10^M \quad (4)$$

$$M = 4.48 \times \left(\frac{V_b}{V_v + V_b} - 0.69\right) \quad (5)$$

where:

N_f = fatigue life (number of design load repetitions to fatigue failure),

ε_h = maximum horizontal tensile strain at the bottom of the bound layer,

$|E^*|$ = dynamic modulus of the asphalt concrete material, psi (use M_R value for asphalt concrete),

V_v = percent air voids volume in total mix, and

V_b = percent binder volume.

The predicted fatigue lives of pavements with control HMA and paving interlayers-treated HMAs are summarized in Figure 3.2. It can be seen that the fatigue lives of pavements with

paving interlayers were higher than that of pavements with control HMA. Fatigue life of pavement with PGM-G100/100 was more than 3 time higher than that of the control HMA.

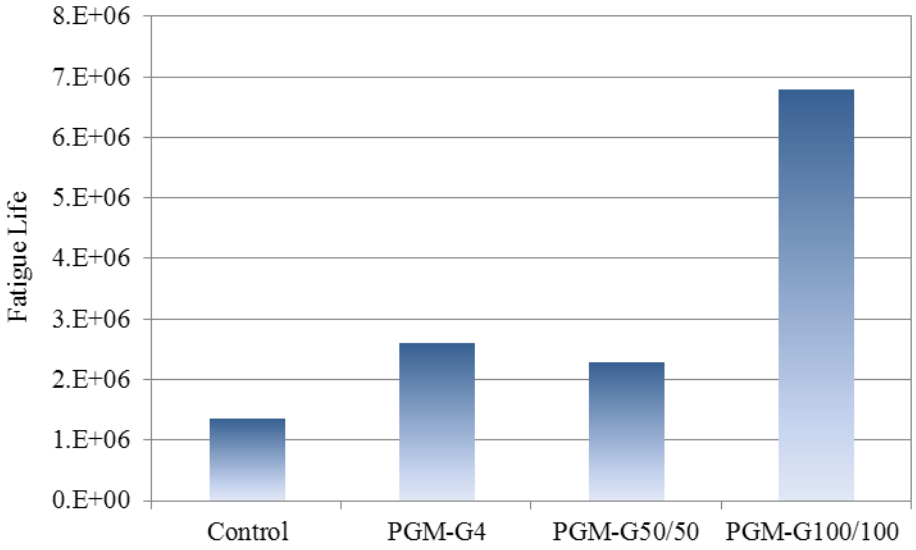

Figure 3.2 Predicted fatigue life

FINITE ELEMENT ANALYSIS

The limitation of the above analyses was that the HMA and the interlayer were considered as one layer. Here finite element method (FEM) was used to simulate responses of different paving interlayer-reinforced AC layers to typical wheel load condition, by considering the HMA and the interlayer as individual layers. ABAQUS - a FEM software package was utilized to facilitate the simulation.

FEM Model Configuration

It is realistic to investigate effects of paving interlayers by simulating a full pavement section. However, due to limited computational resource, such attempt was not successful. Therefore, a small scale paving interlayer-treated pavement was used in this simulation. The model configuration is shown in Figure 3.3. The small-scale pavement was composed of two layers, 2 in of HMA and 2 in of asphalt treated base (ATB). The side length of each slab was 15 in. The paving interlayer was placed between two layers. It was assumed that paving interlayer and asphalt layers were fully bounded, which meant there would not be any relative displacement on the interface. A 90 psi of static load was applied on the top of HMA and the loading zone was a circular area with a radius of 1 in. To simulate the pavement response of reflective cracking, a

crack was assigned through entire ATB and partially at the bottom of HMA. All materials were assumed to be elastic.

Here pavement structure with PGM-G50/50 and PGM-G^4 interlayers are used for comparison. Figures 3.4 and 3.5 show the configuration of fiberglass on PGM-G50/50 and PGM-G^4 interlayers. The space between fiberglass along 45^o direction on G^4 interlayer is not evenly distributed. However, for the convenience of simulation, it was assumed that they were evenly distributed as sketched in Figure 20. The final meshed model is shown in Figure 3.6.

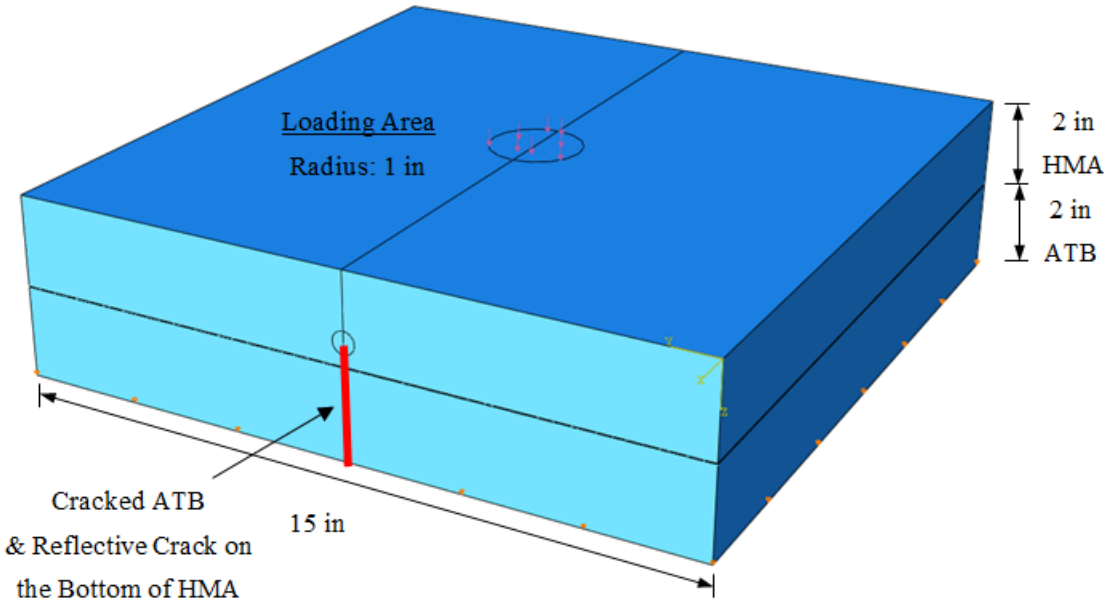

Figure 3.3 FEM model configuration

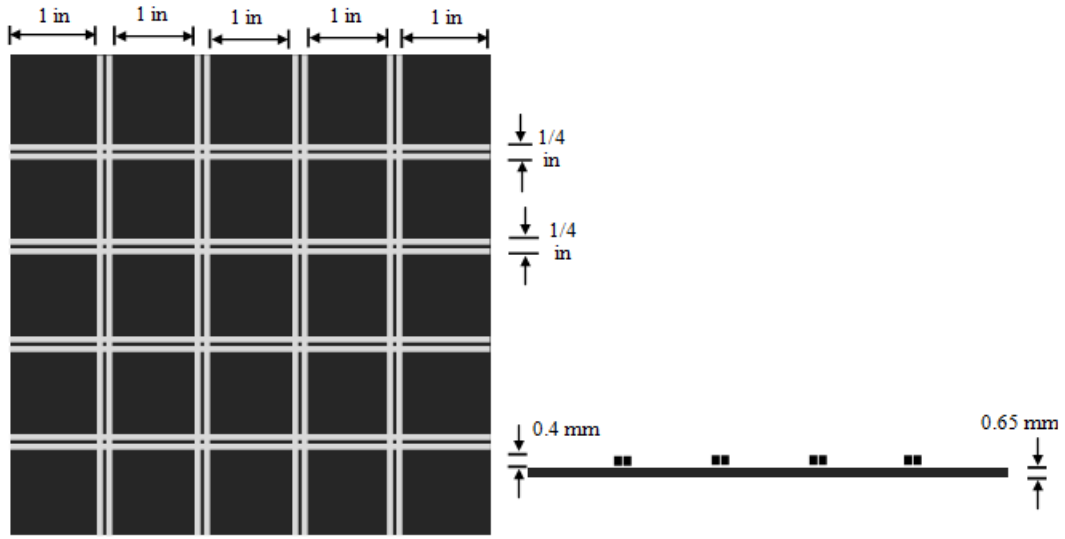

Figure 3.4 Sketch of PGM-G50/50 paving interlayer

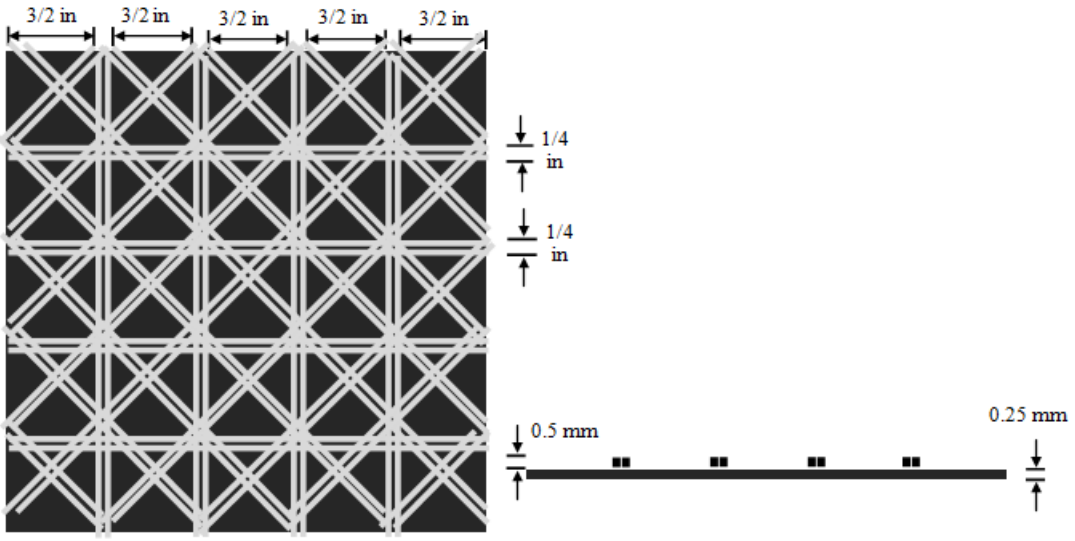

Figure 3.5 Sketch of PGM-G[4] paving interlayer

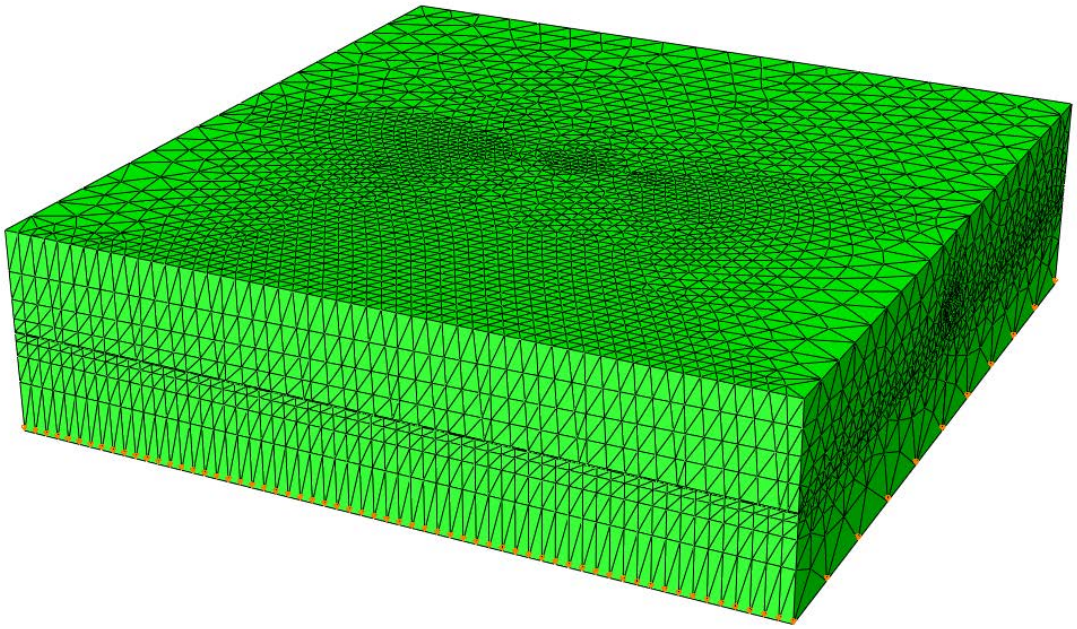

Figure 3.6 Final meshed FEM model

Simulation Results and Analysis

To illustrate the distribution of stress within the pavement, fiberglass was extracted from the calculated FEM simulation results database (Figures 3.7 and 3.8). The stress distribution is illustrated by a color contour. The color scale is on the right of each figure with magnitudes. It can be seen that, the tensile stress along the crack was greater than the rest area for both PGM-G50/50 and PGM-G^4 paving interlayers. However, because of the multi-axial fiberglass configuration, the PGM-G^4 interlayer could be more effective in spreading the load and reducing the maximum tensile stress in the fiber glass.

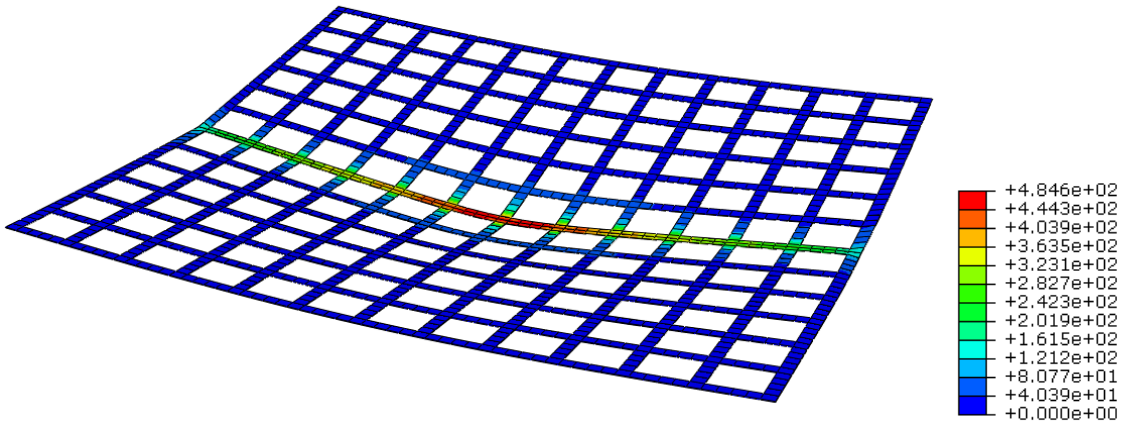

Figure 3.7 Distribution of tensile stress (max principal stress) on the fiberglass of PGM-G50/50

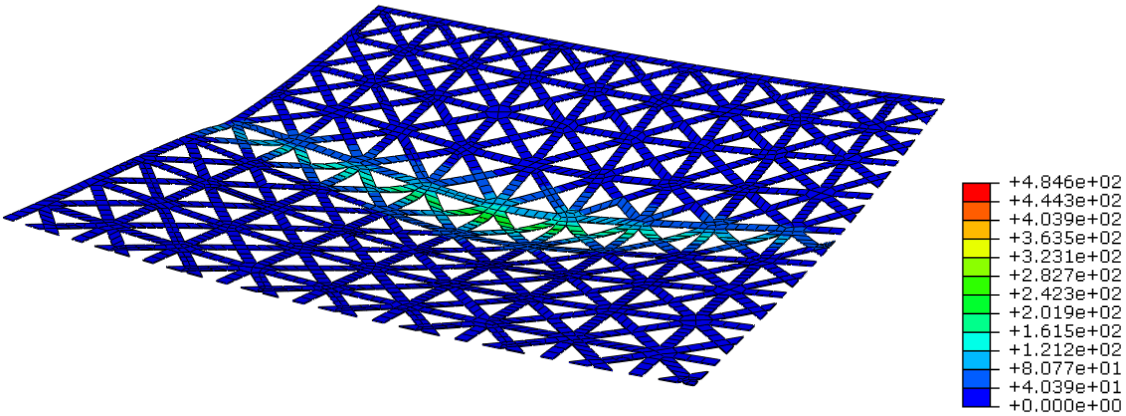

Figure 3.8 Distribution of tensile stress (max principal stress) on the fiberglass of PGM-G^4

The maximum tensile stresses in both paving interlayers are compared in Figure 3.9. The maximum tensile stress in PGM-G50/50 was almost 500 psi and the maximum tensile stress in PGM-G^4 was only about half of that of PGM-G50/50.

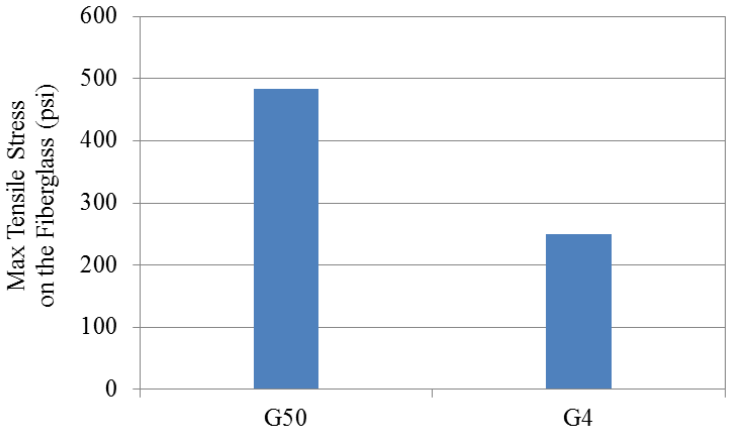

Figure 3.9 Comparison of maximum tensile stress on the fiberglass

The maximum tensile strain at the bottom of HMA layer was often used as a critical pavement response to estimate fatigue cracking in most of pavement design methods. Figure 3.10 compares the maximum tensile strain at the bottom of HMAs with PGM-G50/50 and PGM-G^4 interlayers. The tensile strain of PGM-G^4 treated pavement was significantly lower than that of PGM-G50/50. The tensile strains of PGM-G50/50 and PGM-G^4 reinforced pavements were 521 and 121 microstrains, respectively. Compared to PGM-G50/50, using PGM-G^4 could reduce the maximum tensile strain by 80%.

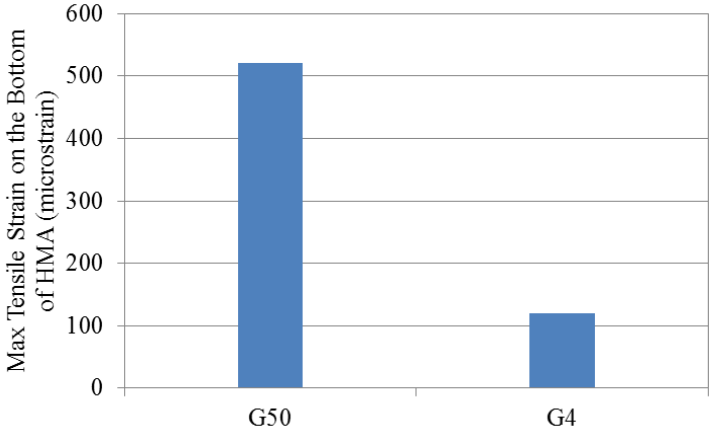

Figure 3.10 Comparison of maximum tensile strain at the bottom of HMA

CHAPTER 4 CONCLUSIONS

The purpose of this study is to explore the application of a multi-axial grid — PGM-G^4 composite interlayer developed by Tencate Geosynthetics in reinforcing AC pavement structures. The study included two phases: laboratory index testing (Phase I) and field performance evaluation (Phase II). This report summarizes work conducted and findings in Phase I, and this chapter presents the conclusions obtained from laboratory tests and data analysis.

Within the scope of this study, conclusions can be drawn as follows.

- Five interlayers were in the following order in terms of asphalt retention value with PG 64-34 binder from highest to lowest one: PGM-G100/100, PGM-G50/50, MPV 500, TruPave®, and PGM-G^4.
- The breaking tensile loads of the saturated and unsaturated paving interlayers in grab strength tests showed that the highest breaking load was obtained on PGM-G100/100, which was mainly contributed by the three yarns of reinforcement fiberglass. PGM-G^4 had the second highest breaking load. All specimens showed an increase of breaking tensile load after saturation and PGM-G^4 had the highest strength increase after saturation.
- The shear test results indicated that optimum performance was maximized when the material was placed "glass-down" into the bitumen tack coat to achieve maximum interface bonding strength.
- Permeability tests were conducted using mixtures reinforced with three interlayers (i.e. PGM-G^4, PGM-G100/100, and PGM-G50/50), with results yielding approximately 1/10 of that of control mixture. The lowest permeability was obtained from PGM-G100/100 treated specimens, followed by PGM-G^4 treated specimens and PGM-G50/50 treated specimens. The permeability of specimens treated by the MPV 500 and TruPave® without tack coat oil was higher than those specimens with tack coat oil, but still lower than the control mixture.
- Interlayer-reinforced mixtures had lower creep compliance than the control mixture. At 20^{o}C, PGM-G^4 treated specimen had the highest creep stiffness, which was doubled that of the control group. The reduction of creep compliance of interlayer treated specimens indicated that the applied load mostly was carried by interlayer and the load on the HMA was reduced. At low temperatures, contraction strain would be generated, especially for locations where cracks exist. Paving composite could provide extra resistance to the thermal contraction. Even after thermal cracks occurred, the asphalt saturated paving interlayer could maintain its integrity.
- The structural analysis based on Bisar program showed that maximum tensile strain in the pavement with paving interlayer was lower than that of pavement with control mix, indicating that using interlayer could improve fatigue crack resistance and extend service life. PGM-G100/100 treated HMA had the lowest tensile strain.

- The calculation of fatigue life (corresponding to the condition of fatigue cracking (bottom-up) covering 45% of the wheel path area) based on the AKFPD program also indicated that the fatigue life of pavements with paving interlayers were higher than that of pavements without an interlayer. The fatigue life of pavement with PGM-G100/100 composite grid was more than three time higher than the control HMA.
- The results from simulation by FEM analysis indicated that the multi-axial fiberglass reinforced paving interlayer PGM-G^4 could improve the stress distribution more effectively than PGM-G50/50. The maximum tensile strain at the bottom of PGM-G^4 treated pavement was only 20% of that of PGM-G50/50 treated pavement.

In summary, the results from Phase I study confirmed that adding a paving interlayer can increase pavement structure stiffness, greatly reduce the permeability and also provide good resistance to low temperature cracking and fatigue cracking. In addition, FEM simulation results indicated that the multi-axial interlayer PGM-G^4 could improve the stress distribution more effectively than bi-axial composite grid as reflected by much lower maximum tensile strain on the bottom of AC layer.

REFERENCES

AASHTO T166 (2008). “Standard Method of Test for Bulk Specific Gravity of Compacted Bituminous Mixes, Using Saturated Surface Dry Specimens”, American Association of State and Highway Transportation Officials,

ASTM, (2004) “Standard PS 129–01 Standard Provisional Test Method for Measurement of Permeability of Bituminous Paving Mixtures Using a Flexible Wall Permeameter”, ASTM International, West Conshohocken, PA.

Button, J. W. (1989). “Overlay Construction and Performance Using Geotextiles”, Transportation Research Record 1248, 24-33.

Chang, D. T., Ho, N., Chang, H., and Yeh, H. (1999). “Laboratory and Case Study for Geogrid-Reinforced Flexible Pavement Overlay”, Transportation Research Record 1687, 125-130.

Chowdhury, A., Button, J. W., and Lytton, R. L. (2009). “Tests of HMA Overlays Using Geosynthetics to Reduce Reflection Cracking”, FHWA/TX-10/0-1777-3, Texas Transportation Institute, the Texas A&M University System, College Station, TX.

Department of Transportation State of Georgia, (2011) GDT 1, www.dot.ga.gov/doingbusiness/TheSource/gdt/gdt001.pdf

G. W. Maupin, Jr. (2000). “Investigation of Test Methods, Pavements, and Laboratory Design Related to Asphalt Permeability”, Virginia Transportation Research Council, Charlottesville, VA.

Khodaii, A., and Fallah, S. (2008). “The Effect of Geogrid on Reduction of Reflection Cracking in Asphalt Overlay”, the 4th National Conference on Civil Engineering, University of Tehran.

Saraf, C. L., Majidzadeh, K., and Tribbett, W. O. (1996). “Effect of Reinforcement on Fatigue Life of Asphalt Beams”, Transportation Research Record 1534, 66-71.

APPENDIX: JMF of Rich Hwy North Pole Interchange Paving Project

STATE OF ALASKA - NORTHERN REGION
DEPARTMENT OF TRANSPORTATION AND PUBLIC FACILITIES
BITUMINOUS MIX DESIGN MARSHALL METHOD
2301 PEGER ROAD
FAIRBANKS, AK 99709

RECEIVED: 6/18/2008
COMPLETE: 5/25/2008

PROJECT NAME:	Rich Hwy North Pole Interchange	REGIONAL LAB # :	08-246
PROJECT NUMBER:	ACIM-0A2-4(26)	FIELD # :	NPI-HMA-MD-1
LEDGER CODE:	30388942 / 62184	TYPE/CLASS:	II B

AGGREGATE SOURCE:	900 Old Rich
AGGREGATE QUALITY#:	06-067
BLEND RATIO:	23:23.5:42:11.5 CA:INT:FA:SA
BLENDED BULK SPG:	2.677
EFFECTIVE SPG:	2.706

BINDER SOURCE:	EPA
BINDER GRADE:	PG 64-34
BINDER SPG:	1.0016
ANTISTRIP:	.25%

MIX DESIGN PARAMETERS	
STABILITY	1200
FLOW	8-16
VOIDS TOTAL MIX	3-5
COMPACTION, BLOWS	50
VOIDS FILLED	65-78
VMA	12
DUST RATIO	.6-1.4

MIXING TEMP (DEG F)	302
COMPACTING TEMP (DEG F)	295

MARSHALL RESULTS	
% ASPHALT @ MAX UNIT WT	6.5
% ASPHALT @ MAX STABILITY	6
% ASPHALT @ 4% VOIDS	5.4
OPTIMUM OIL CONTENT = 5.4 %	
STABILITY	2375
FLOW	9.7
VOIDS TOTAL MIX	4
VOIDS FILLED	74
VMA	16
MTD/RICE	2.483
DUST ASPHALT RATIO	0.7

APPROVED:

AGGREGATE DESIGN PARAMETERS		
		Spec
F&E	0%	8%max
LL	NV	
PI	NP	
T304		
FRACTURE	98%	90%df

SIEVE SIZE	PROPOSED GRADATION	MIX DESIGN SPEC BAND	
		LSL	HSL
1"		-----	-----
3/4"		-----	-----
1/2"	87	81	93
3/8"	74	68	80
#4	52	46	58
#8	39	33	45
#10		-----	-----
#16	30	25	35
#20		-----	-----
#30	25	21	29
#40		-----	-----
#50	19	15	23
#60		-----	-----
#80		-----	-----
#100	8	5	11
#200	3.5	1.5	5.5

REMARKS:

Performance of Tencate Mirafi PGM-G^4 Interlayer-Reinforced Asphalt Pavements in Alaska

Phase II Report

Submitted to
Tencate Geosynthetics North America

by

Jenny Liu, Ph.D., P.E.
Professor
Department of Civil and Environmental Engineering

Sheng Zhao, Ph.D
Research Associate
Center for Environmentally Sustainable Transportation in Cold Climates

Paul Eckman
Undergraduate Research Assistant
Department of Civil and Environmental Engineering

August 2015

University of Alaska Fairbanks
Fairbanks, AK 99775-5900

TABLE OF CONTENTS

LIST OF FIGURES

LIST OF TABLES

INTRODUCTION

Paving interlayers have been used in asphalt overlays in a variety of design and construction situations for more than three decades. In *Phase I* of the project, *Performance of Tencate Mirafi PGM-G^4 Interlayer-Reinforced Asphalt Pavements in Alaska*, several types of paving interlayers provided by Tencate Geosynthetics were used to explore the performance of paving interlayers reinforced asphalt concrete (AC) pavements in Alaska. Laboratory testing and finite element method (FEM) simulation identified a number of engineering benefits of using paving interlayers in AC pavements. To further validate performance of paving interlayers in AC pavements in the field, the research team at the University of Alaska Fairbanks coordinated with AKDOT&PF Northern Region personnel to select a pavement preservation/rehabilitation project (using thin AC overlay) constructed during summer construction season for establishment of test sections. The field related activities compose Phase II of the project, including pre-construction field evaluation, establishment of test sections and field evaluation after construction.

TEST SITE DESCRIPTION

The project starts from MP148 on the Richardson Highway. The roadway consists of 2 inches HMA, 4 inches ATB, 4 inches D-1 granular material and about 3 feet selected material. The selected material was crushed rock from the paving site. The first lift of 2 inches was paved in the fall of 2012.

PRE-CONSTRUCTION FIELD EVALUATION

A pre-construction field evaluation was conducted in May 2013. Cracks were observed on paved asphalt treated base (ATB) after snow melted away from roadway surface. The problematic areas were at 1.4 mile to 6.7 mile from the beginning of paving project. Most problematic areas had weak foundation and most cracks were longitudinal cracks. 12 cracking areas (Figures 1-13) were identified and the detailed information is presented in Table 1.

Table 1 Summary of pre-construction pavement survey

ID	Mileage	Location	Length (ft)	Note	Suggestion
1	1.4	Longitudinal, Left lane, in the middle	169		Can be used as a fabric test section. A 6 ft. wide fabric can cover the cracking area.
2	1.6	Longitudinal, mostly in the right lane,	172	Weak foundation	
3	1.7	Longitudinal, right lane,	105	Weak foundation, some on the shoulder	
3a	1.7	Longitudinal, right lane,	158	Weak foundation, some on the shoulder	
4	1.8	Longitudinal, right lane	283		Can be used as a control section
5	1.9	Longitudinal, right land	191	On the shoulder	Not suggested as a test section, since it is on the shoulder.
6	2.1	Longitudinal, left lane	142		Can be used as a fabric test section, which needs a 12 ft. wide fabric.
7	3.5	Longitudinal, left lane	386	most of the crack is on the longitudinal joint	
8	3.6	Longitudinal, left lane	247	including one transverse cracking	Can be used as a fabric test section. It needs a 12 ft. wide fabric.
9	3.8	Longitudinal, left lane	245		Can be used as a fabric test section. It needs a 6 ft. wide fabric.
10	4.1	Longitudinal, left lane	478		Can be used as a control section and a fabric test section next to each other for comparison. It needs a 12 ft. wide fabric.
11	4.8	Longitudinal, right lane	293	on the shoulder	Not suggested as a test section, since it is on the shoulder.
12	6.7	Longitudinal, left lane close to joint	157		

Figure 1 Cracking area 1

Figure 2 Cracking area 2

Figure 3 Cracking area 3

Figure 4 Cracking area 3a

Figure 5 Cracking area 4

Figure 6 Cracking area 5

Figure 7 Cracking area 6

Figure 8 Cracking area 7

Figure 9 Cracking area 8

Figure 10 Cracking area 9

Figure 11 Cracking area 10

Figure 12 Cracking area 11

Figure 13 Cracking area 12

ESTABLISHMENT OF TEST SECTIONS

Three test sections reinforced with paving interlayers were established in July, 2013: one with G^4 in areas 2 and 3 (Figure 14), one with G50/50 in area 9 (Figure 15), and one with G100/100 in area 10 (Figure 16). A tack coat of neat oil was applied at the shooting rates of 0.19 gal/yd^2, 0.27 gal/yd^2, and 0.27 gal/yd^2 for sections with G^4, G50/50 and, G100/100 respectively. Area 4 was selected as the control section without paving interlayers.

Figure 14 G^4 test section

Figure 15 G50/50 test section

Figure 16 G100/100 test section

FIELD EVALUATION AFTER CONSTRUCTION

Field Surveys in August and October, 2013

Two pavement condition surveys were conducted on August 19 and October 12, 2013. No cracks were found in any of the test sections during these two field trips (Figures 17-20).

Figure 17 Control section (300 feet in area 4)

Figure 18 G^4 test section (reinforced with 300 feet of G^4 paving interlayer in the right lane in area 2, no visible cracks)

Figure 19 G50/50 test section (reinforced with 300 feet of G50/50 in the left lane in area 9, no visible cracks)

Figure 20 G100/100 test section (reinforced with 300 feet G100/100 in the left lane in area 10, no visible cracks present)

Field Survey in May 2014

A field evaluation was performed on May 15th, 2014 to see how the paving interlayers have functioned over the course of the winter. Cracks were observed in every test section (Figures 21-24) and Table 2 summarizes crack data collected.

Table 2 Summary of crack data in May 2014

Section	Transverse crack (#)	Longitudinal crack, NB (ft)	Longitudinal crack, SB (ft)
Control (area 4)	0	266 medium-major	0
G^4 (areas 2 & 3)	3 minor	17 minor	0
G50/50 (area 9)	1	-	36 minor
G100/100 (area 10)	1	-	0

(a)

(b)

Figure 21 Control section: a) no visible cracks (October 12, 2013); b) 266 feet of longitudinal cracking (May 15, 2014)

(a)

(b)

Figure 22 G^4 test section: a) no visible cracks (October 12, 2013); b) both longitudinal and transverse cracks present (May 15, 2014)

(a)

(b)

Figure 23 G50/50 test section: a) no visible cracks (October 12, 2013); b) both transverse and longitudinal cracking present (May 15, 2014)

(a)

(b)

Figure 24 G100/100 test section: a) no visible cracks (October 12, 2013); b) transverse cracking present (May 15, 2014)

The control section (area 4) was the worst with 89% of the northbound lane carrying a 266-ft medium severity longitudinal crack. The northbound lane of area 2 that was reinforced with G^4 paving interlayer had one full length transverse crack and two others that started from the shoulder and crossed the northbound lane ending at the centerline. There were also small transverse cracks between 274-294 feet from the start of G^4 section in the center of the northbound lane. The southbound lane of area 9 is the section reinforced with G50/50. There was a transverse crack at 160 feet from the start of G50/50 section. The first part of southbound lane of area 10 is the 300-feet G100/100 reinforced section. There was only one full length transverse crack located about 117 feet from the start of the reinforcement.

According to the summary in Table 2, all sections reinforced with paving interlayers showed better pavement performance (reduced amount and severity of cracking) than the control section. In terms of number and severity level of cracks, section reinforced with G100/100 performed the best, followed by G^4 section, and G50/50 section. That G^4 section showed more cracks than G100/100 section may be due to the weak foundation in areas 2 and 3 where G^4 section was located. In addition, another observation from the pavement survey was many of the transverse cracks were located at the possible interlayer joints. During the construction of test sections, all paving interlayers were cut to pieces of about 300-ft long for easy installation, which may cause the weak spot for stress concentration and crack occurrence in the interlayer sections. It could be avoided in real construction while paving interlayers are laid out continuously as an entire layer.

Field Survey in September 2014

The G^4 reinforced section (area 2) had the only new crack found in all of the test sections and it was minor (Figure 25-27). There were many very small fissures where it was likely that after the next winter more cracks would become pronounced. Overall the test sections including the controls were in the same condition as the last evaluation.

Figure 25 Control section (area 4) no new cracking

Figure 26 G^4 section (area 2) new minor cracking

Figure 27 G50/50 and G100/100 (sections 9 and 10) no new cracking

Field Survey in June 2015

A field evaluation was performed with crack data collected on June 2nd, 2015. The crack data collected from the survey conducted in May 2014 and this survey is summarized and presented in Table 3. Figures 28 to 31 show the typical new cracks in every test section.

Table 3 Summary of crack data in June 2015

Section		Transverse crack (#)	Longitudinal crack, NB (ft)	Longitudinal crack, SB (ft)
Control (area 4)	Previous	0	266 medium-major	0
	New	7 minor	34 medium-major 13 minor	0
	Total	7 minor	300 medium-major 13 minor	0
G[4] (areas 2 & 3)	Previous[1]	3 minor	17 minor	0
	New[2]	5 minor	46 minor	14 minor
	Total	8 minor	63 minor	14 minor
G50/50 (area 9)	Previous	1 major	0	36 minor
	New	0	50 minor	24 minor
	Total	1 major	50 minor	24 minor
G100/100 (area 10)	Previous	1 major	0	0
	New	0	0	0
	Total	1 major	0	0

[1] *Previous−Data collected in May 2014.*

[2] *New−Data collected in June 2015.*

(a)

(b)

Figure 28 Control section: a) new minor transverse cracking; b) new moderate-major longitudinal cracking

(a)

(b)

Figure 29 G^4 test section: a) new minor transverse cracking; b) new minor longitudinal cracking

(a)

(b)

Figure 30 G50/50 test section: a) no new transverse cracking; b) new minor longitudinal cracking

(a)

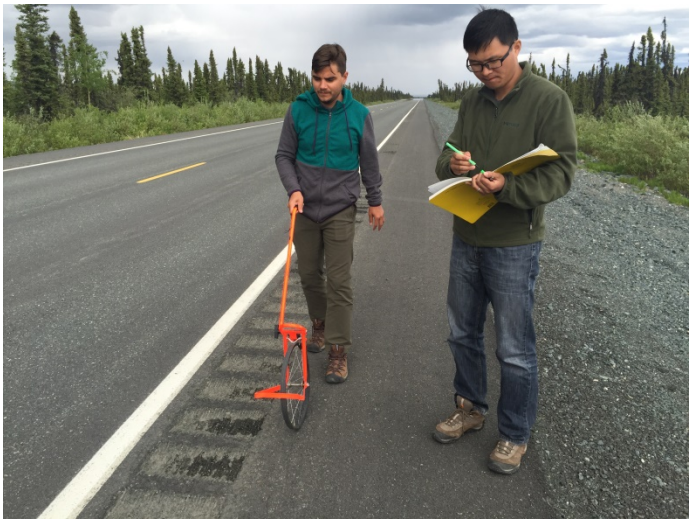

(b)

Figure 31 G100/100 test section: a) no new transverse cracking; b) no new longitudinal cracking

According to Table 3, it can be seen that the control section showed the worst longitudinal cracking performance in terms of new crack amount and severity after one year's service. In addition, most new transverse cracks were found on control section compared to sections reinforced by paving interlayers. The G^4 reinforced section showed several newly formed minor transverse and longitudinal cracks, while new minor longitudinal cracks were observed on the G50/50 section only. The G100/100 section performed the best without any new cracks observed.

As discussed previously, more cracks observed on the G^4 section than G100/100 section may be due to the weak foundation in areas 2 and 3 two where G^4 section was located. It should also be noted that plenty of transverse cracks were found at the possible joints caused by each 300-ft paving interlayer during construction. The stress concentration at the joints may have caused the

cracks other than the effects of paving interlayers. These factors may have affected the surveys conducted in this study but could be avoided in real construction.

SUMMARY AND RECOMMENDATION

After two years' surveying and monitoring, it can be observed that all test sections reinforced with paving interlayers showed better pavement performance than the control section. This means that the placement of paving interlayers selected in this study would benefit the pavement performance. Among the sections with paving interlayers built in, the G100/100 reinforced pavement showed the best performance, followed by G50/50 reinforced section, then the G^4 section.

However, it is still too early to draw any conclusion about the paving interlayer effects, as two years are typically considered a short period in the entire life cycle of a pavement. In addition, a few construction issues were noticed that may have affected the survey results. Therefore, it is our recommendation that field cores be collected from the sites at which the cracking occurred, in order to reveal more information underground. It is also recommended that we continue to monitor the test sections with more detailed description of the pavement distresses to see how they progress with time. Having a few more years' data would give a much clearer projection of the utility of the paving interlayers in cold regions.